Chapter 2
Hydrothermal synthesis and characterization

2.1 Hydrothermal procedure

Hydrothermal synthesis can be defined as reactions occurring under the conditions of high-temperature–high-pressure (above 100°C and 1 atm) in aqueous solutions in a closed system [22]. According to this result, hydrothermal synthesis takes place at elevated temperature (>100°C) and pressure (greater than atmospheres) . It usually relates to water as a catalyst and sometimes as a component of solid phases in the synthesis [2 0] . Hydrothermal synthesis of TiO_2 involves self-assembly which is nanofabrication approach by bottom-up self-construction of atoms smaller than a nanometer and autonomously grows into nanostructures [2 1] . Self- assembly is any spontaneous formation of an organization from individual parts without human intervention, which takes place in liquid phase. Self- assembly is the product of interaction of interfacial forces that reactants undergo chemical change at interface on the surface of solid. The ordered formation is usually the result of equilibrium state (influenced by appropriate environment or hydrothermal condition) , which individual parts keep equal distance to each other, not a random aggregation [22]. Crystallization routes have been explored that concern the use of pattern and electrostatic interactions that assist self-organization of crystalline into desired geometries. Therefore, bottom-up architectures of nanostructures need to govern over the nucleation and assembly of first precipitates. Rutile structure rises from oriented assembly of Ti(IV) -butoxide (TBO) precursor [21].

Hydrothermal method is preferential compared to other techniques. For the system involved high pressure in autoclave, then a single crystal and polycrystalline can be produced at low temperature (<250°C), which do not require a sintering process at high temperature. Furthermore, the equipment and methodologies are simple and proper for low cost manufacturing [4 , 1 9] . In this work, TiO_2 NRs will be prepared via the hydrothermal method on FTO substrate assisted by TiO_2 seed layer. However, the characteristics of TiO_2 NRs depend not only on the seed layer but are also influence by hydrothermal parameters such as precursor concentration (Titanium (IV) butoxide) and

ลิขสิทธิ์มหาวิทยาลัยเชียงใหม่
Copyright© by Chiang Mai University
All rights reserved

synthesis time. This process can vastly influence the crystallinity and growth orientation of TiO_2 films.

2.2 Material characterization

2.2.1 Crystal structure of TiO_2

Structural information of compounds can be identified by x-ray diffraction (XRD) technique. The XRD analysis provides information of crystalline material in range of unit cell dimensions. X-rays are form of electromagnetic radiation with a short wavelength. X-rays are used to produce the diffraction pattern because their wavelength λ (0.01-10 nm) is small as the spacing *d* between planes in the crystal [23]. X-ray reflection pattern is characteristic form of individual material. When an incoming X-ray beam strikes an atom, the electrons around the atom begin to oscillate with the same frequency as the x-ray beam. The incoming beam travels in almost all directions resulting in destructive wave combination. Hence, there is no energy releasing from the solid sample. However, the atoms in a crystal are aligned in an ordered orientation, x-ray beams pierce through the sample at difference directions. Thus, a diffracted beam can be considered as interference of a large number of scattered [24]. Bragg's law represents the relation between lattice spacing (*d*-spacing) and x-ray wave length as Eq. (2.1). The determination of plane spacing (d-spacing) can be accomplished by Bragg's law as;

$$2d \sin\theta = n\lambda, \tag{2.1}$$

ลิขสิทธิ์มหาวิทยาลัยเชียงใหม่
Copyright© by Chiang Mai University
All rights reserved

where λ is wavelength of the X-ray, θ is scattering angle, n is a positive representing the order of the diffraction peak, and d is inter-plane distance of atoms.

The physical properties of TiO_2 are significantly dependent on the crystal structure. At ambient condition, TiO_2 has two dominant phases as rutile and anatase. Both structures are tetragonal lattice that constructs from octahedral building blocks consisting of chains of TiO_6 octahedra. Ti^{4+} ion is surrounded by an octahedron of six O^{2-} ions. The two crystalline forms both anatase and rutile TiO_2 consist of TiO_6^{2-} octahedral. In the rutile phase, two opposite edges of each octahedron link at a corner of

oxygen atom, forming linear chains of octahedral at corner. On the other hand, anatase has no corner sharing but shows four edges shared per octahedron (faces sharing). The anatase structure consists of zigzag chains of TiO_6^{2-} octahedral links to each other with edge-sharing bonding. Because anatase has more edge sharing, the internal spaces between octahedra are larger (as in Figure 2.1) resulting in less density packing than rutile [25-27].

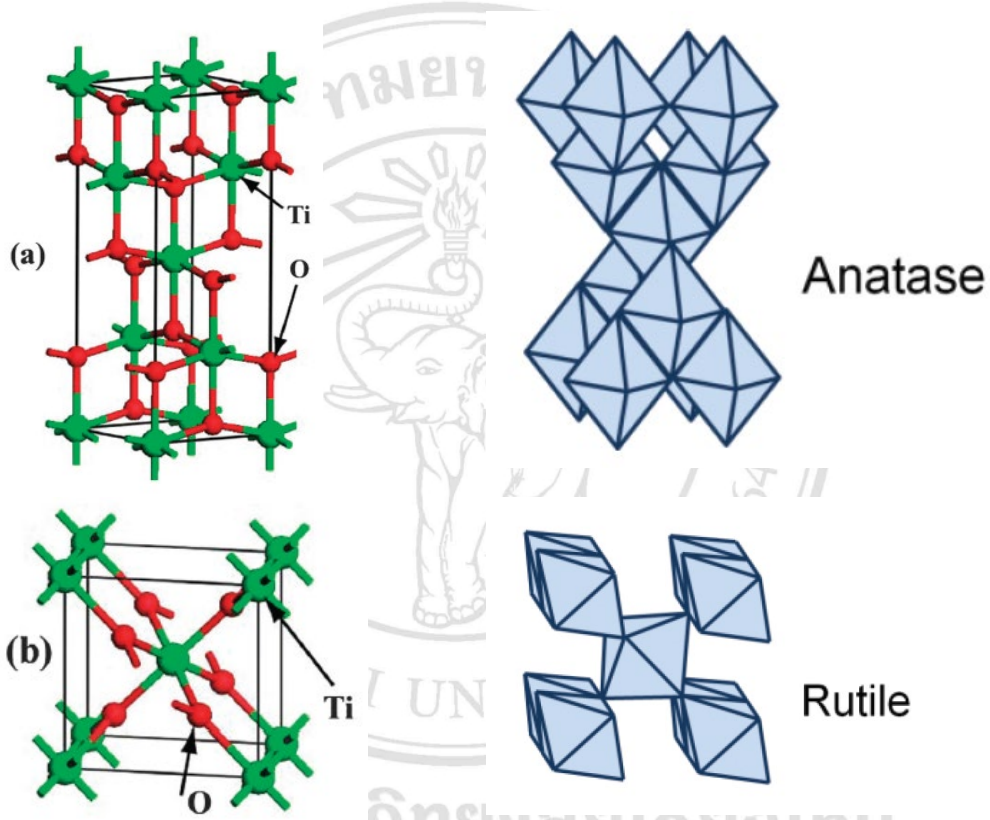

Figure 2.1 Molecular structures of TiO_2 (a) rutile and anatase (b) [28, 29]

ลิขสิทธิ์มหาวิทยาลัยเชียงใหม่
Copyright© by Chiang Mai University
All rights reserved

2.2.2 Energy band of TiO_2

In quantum mechanical system, energy of electrons in an atom is discrete energy level or quantized energy level. Electrons always travel around nuclei all the time so determination of electron position can specify by electron probability density. If all atoms are isolated, the electron energy will separate from each other by a large distance. When the atoms get closer, wave functions of outer electrons start to overlap to each other's. Therefore, electron probability density interacts with the neighboring atoms resulting in electron energy level (which is quantized for single atoms) splitting

out to be several energy levels. Regarding to Pauli Exclusion Principle, electrons cannot occupy the same quantum state within a quantum system, thereby electrons have different quantum states by separation of electron energy level. The small states occur called energy band consisting of allowed band which electrons can occupy and forbidden band. This model used to describe conductivity in semiconductor. For semiconductor at 0 K, the high allowed band usually free of electrons which is the empty state named conduction band (CB) and the low band that fill of electrons (filled state) is valance band (VB). The different between the lowest CB and highest VB is forbidden band or energy gap (E_g). The filled state (VB) cannot conduct electricity because electron cannot transfer.

For high temperature or activation of light, energy at least equal to E_g can promote electrons to change state from VB to CB and left hole at VB. Movement of electron in CB and hole in VB induced electric current in semiconductor [30]. Hence, semiconductor requires photon energy more than its E_g to create one electron-hole pair as follows:

$$E_g = h\upsilon, \tag{2.2}$$

where $h = 6.626\times10^{-34}$ J□s is the Planck constant and υ is frequency of photon.

The crystal structures, band structures, density of states (DOS) of anatase and rutile TiO_2 were calculated by first-principles density functional theory (DFT). The results demonstrate that both of TiO_2 valence bands comprise of O 2p states and a few Ti 3d states. The strong p–d hybridizations between O 2p and Ti 3d states which establish bonding states in the valence band contribute to transfer of photoexited holes. Moreover, the conduction bands mainly consist of Ti 3d states with a few O 2p and Ti 3p states and the present of strong hybridization exists between Ti 3d and O 2p as shown in Figure 2.2 [28]

ลิขสิทธิ์มหาวิทยาลัยเชียงใหม่
Copyright© by Chiang Mai University
All rights reserved

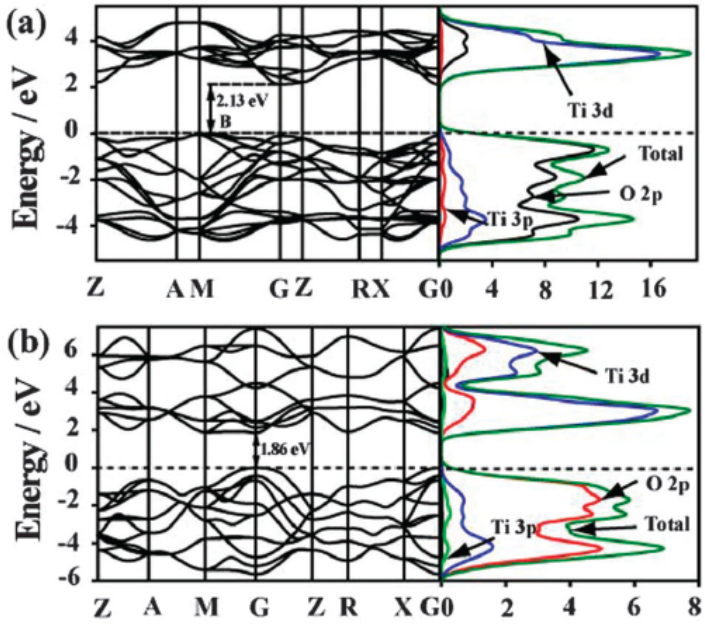

Figure 2.2 The DOS and band structures of anatase (a) and rutile (b) TiO_2 with Fermi level shown by a dashed line [28]

The energy band structures of anatase and rutile were calculated by DFT. Band gap energies were observed between the conduction band minimum (CBM) and the valence band maximum (VBM). Anatase exhibits an indirect band gap of 2.13 eV and rutile is a direct band gap semiconductor with 1. 86 eV band gaps. Although both methods have the same tendency, the calculated values are much smaller compared to the experimental values (3.2 for anatase and 3.0 for rutile) [26]. Since anatase possess the long electron lifetime which is higher than 1 μs, more than 10 μm electron diffusion length can be observed, which is much longer than those in rutile (100-650 nm) , calculated by the electron mobilities of 20 and 0. 1 cm^2/ Vs in rutile and anatase, consequently. This long diffusion length could raise the light-harvesting efficiencies and photocatalytic reactivity in anatase [5, 29].

To determine the energy band, ultraviolet–visible spectroscopy (UV-VI) can be used. UV-VIS is the measurement of the intensity of light after penetrates through a sample or after reflection from a sample surface. To observe optical properties of material such as the light absorption, a single wavelength or over a continuous spectral range light can be used for measurement. The limits of detection are approximately 170–1100 nm for silicon-based detector. Absorption of ultraviolet spectra contributed to

ลิขสิทธิ์มหาวิทยาลัยเชียงใหม่
Copyright© by Chiang Mai University
All rights reserved

transfer outer electrons of atoms absorbing photon energy to higher energy state because adsorption of photon can be converted into atoms energy and cause atoms energy change into higher level. The difference of energy change can be examined by measurement of light energy before and after piece through a sample. The absorbed energy is to raise the molecule from the ground state energy E_0 to the higher excited state (energy E_1). The difference in energy is given by

$$\Delta E = E_1 - E_0 = h\upsilon = h\frac{c}{\lambda}, \tag{2.3}$$

where h = Planck's constant, c = velocity of light, λ = wavelength of the absorbed radiation and υ is frequency of molecule absorbed ultraviolet radiation. Absorption degree of a sample is recorded by a spectrometer at different wavelengths causing plot of absorbance (α) in various wavelength (λ) [31]. E_g can be calculated as follows:

$$\alpha = \frac{1}{d}\ln(\frac{1}{T}), \tag{2.4}$$

$$\alpha h\nu = A\left(h\nu - E_g\right)^n, \tag{2.5}$$

where α is absorption coefficient, d is thickness of nanorods, T is transmittion coefficient, A is a constant, and n is $1/2$ for direct allowed transition (2 for indirect allowed transition).

ลิขสิทธิ์มหาวิทยาลัยเชียงใหม่
Copyright© by Chiang Mai University
All rights reserved

2.3 Charge recombination mechanism

The carrier recombination dynamics in rutile and anatase TiO_2 single crystals were studied by combining time-resolved, transient absorption and photoconductivity measurements. In rutile, the electrons and holes show exponential decays with lifetimes of 24 and 48 ns, respectively. In contrast, anatase illustrates non-exponential decay. Electrons appear in the conduction band for more than a few microseconds, while holes promptly decrease within a few nanoseconds [29].

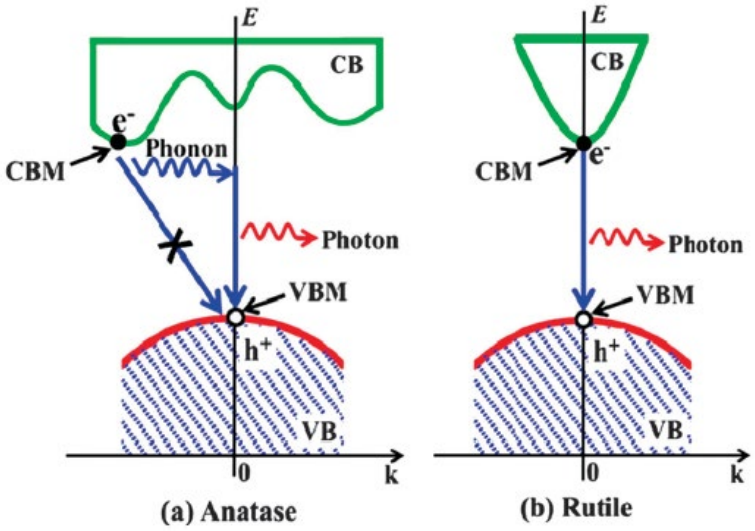

Figure 2.3 Recombination processes of photoexcited electrons and holes within indirect gap anatase and direct gap rutile (b) [28]

Carrier recombination occurs when excited electron in conduction band moves backward to recombine with photoexcited hole and emitting energy. Therefore, electron has low energy and returns to valance band. When the electrons come back from the conduction band to the valence band, extra energy will be released as photons. Moreover, the excited electrons must obey the transition selection rule of momentum conservation; referring to the following:

$$E_g = \hbar\omega, \tag{2.6}$$

$$\hbar\mathbf{k}'_e - \hbar\mathbf{k}_e = \pm\hbar\mathbf{q}_{\text{phonon}}, \tag{2.7}$$

where $\hbar$ is the reduced Planck constant, $\mathbf{k}'_e$ and $\mathbf{k}_e$ are the electron wave vectors at the VBM and CBM, respectively, $\mathbf{q}_{\text{phonon}}$ is the wave vector of the assisted phonon, E_g is the band gap of semiconductor, and ω is angular frequency of the emissive photon.

For recombination of rutile, an electron only emits a photon because in the direct band gap semiconductors (CBM and VBM are in the same position). However, in the indirect band gap semiconductors as anatase, excited electron require assistance from phonon to recombine with hole. Hence, the photogenerated electrons cannot recombine with holes readily, resulting in higher exited electron–hole lifetime in anatase compared with rutile [26]. as shown in Figure 2.3 [28].

ลิขสิทธิ์มหาวิทยาลัยเชียงใหม่
Copyright© by Chiang Mai University
All rights reserved

2.4 Growth mechanisms of TiO_2 NRs

Generally, formation of TiO_2 NRs by hydrothermal procedure is conducted in hydrochloric acid (HCl) diluted with deionized water (DI) and Ti(IV)-butoxide (TBO) applied as a reactant with structure formula $Ti(OCH_2CH_2CH_2CH_3)_4$. There is a number of approaches explained growth mechanisms of TiO_2, which are interesting and beneficial explanation for this research.

When the four-fold Ti precursor ($[Ti(RO)_4]$) reacts with water, the coordination number of Ti^{4+} increases from four (+ 4) to six (+ 6) to accept oxygen lone pairs formimg Ti-O bond. These six-fold structural units obtain high pressure and become the octahedra that finally combine into the precipitate crystal. The octahedra agglomeration grows along corner and edge sharing during the condensation reactions. During the particle agglomeration, the acidity of the reaction solution plays a crucial factor for the hydrolysis of $Ti(ROH)_4$ in aqueous solution [21]. Under high acidity, Ti-OH^- groups receive H from HCl and turn into Ti-OH_2^+ groups (protonated groups) that easily combine with OH^- groups of other TiO_6 octahedra (Figure 2.4). The hydrogen bond among the protonated nanocrystallines could attribute to aggregation of TiO_2. To form Ti–O–Ti oxygen bridge bonds, water molecule is eliminated (dehydration) [32]. Rutile phase requires high degree of protonation of the TiO_6 octahedra to form their favorable dense orientation. That means it desires advanced acid intensity to effective catalyze the hydrolysis and dehydration reaction. Furthermore, the crystal growth must precede through high temperature. Whereas, formation of the anatase phase preferred weak acid conditions because of the lower surface energy of anatase compared with that of rutile. [21]. After dehydration reaction, poor protonation process results in face-sharing anatase phase (Figure 2.5 (a)) while sufficient protonation results in corner and edge sharing (Figure 2.5 (b))..

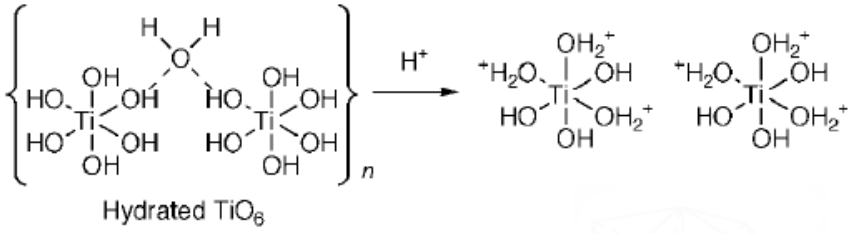

Figure 2.4 Formation of the TiO_6 octahedra from protonation [32]

ลิขสิทธิ์มหาวิทยาลัยเชียงใหม่
Copyright© by Chiang Mai University
All rights reserved

Chemical reaction of hydrolysis process and dehydration (condensation) in hydrothermal synthesis can be written as follows [29]

Hydrolysis $$\mathrm{Ti(OR)_4 + 4H_2O \rightarrow 2Ti(OH)_4 + 4ROH} \quad (2.8)$$

Dehydration: $$\mathrm{Ti(OH)_4 + Ti(OH)_4 \rightarrow 2TiO_2 + 4H_2O} \quad (2.9)$$

$$\mathrm{Ti(OH)_4 + Ti(OR)_4 \rightarrow 2TiO_2 + 4ROH.} \quad (2.10)$$

The entire reaction via the hydrothermal process between TBO precursor and water is [21]

$$\mathrm{Ti(OR)_4 + 2H_2O \rightarrow TiO_2 + 4ROH,} \quad (2.11)$$

where R is the component of Ti(IV) -butoxide named butyl-group with the general formula C_4H_9. Concentrations of acidity (OH^- / H^+ ratio) are crucial for crystal orientation. Recently, the similar hydrothermal approach with the resembling hydrothermal solution using TBO, HCl and DI water, reported that the present of maximum oxygen in TiO_2 was observed by XPS. This maximum comes from OH and OH_2 groups. While the surface hydroxide ions contribute to the 1D growth of single crystalline TiO_2 nanorods on FTO substrate [33]. Another report indicated that anatase and rutile phase are the results from nanorods synthesis on seed layer by hydrothermal method using 4-5 pH and 1-2 pH synthesis solutions, respectively [19].

ลิขสิทธิ์มหาวิทยาลัยเชียงใหม่
Copyright © by Chiang Mai University
All rights reserved

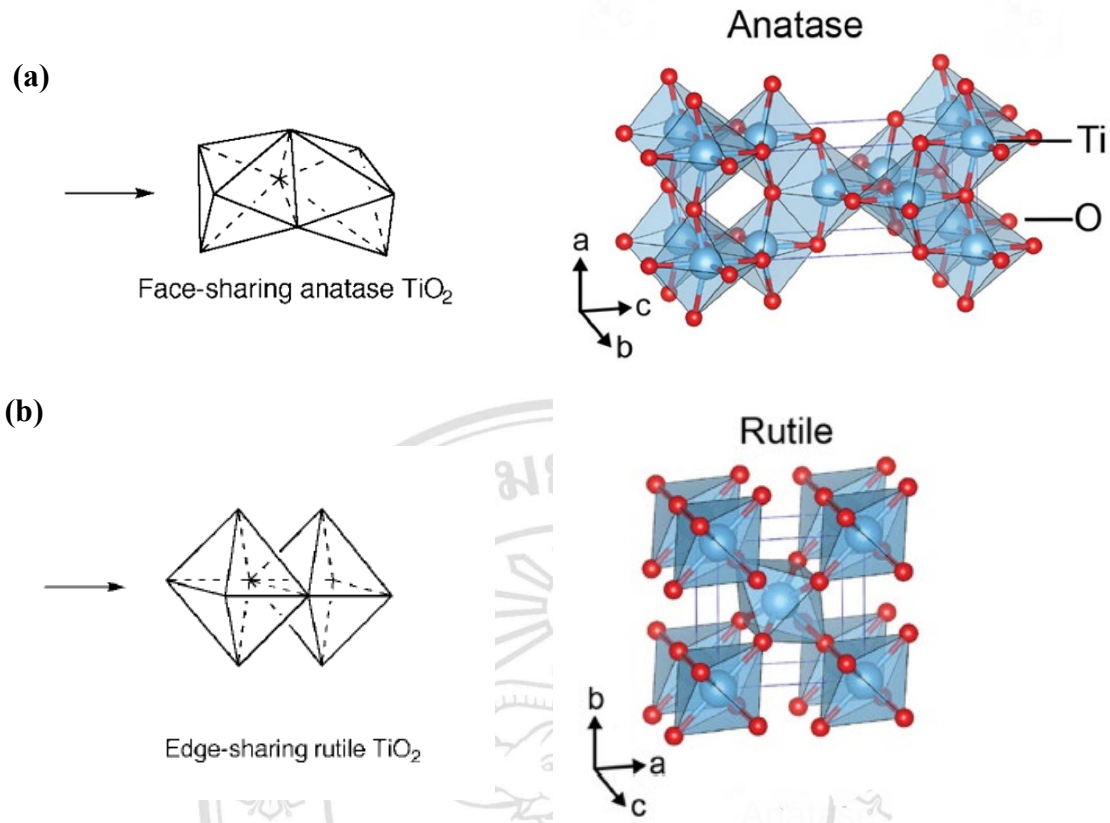

Figure 2.5 (a) Face-sharing octahedra of anatase (b) and edge-sharing octahedra of rutile [32, 34]

Moreover, other purpose of growth mechanisms showed that Ti rapidly reacts with HCl vapor to produce unstable Ti^{3+}, and then Ti^{3+} is promptly hydrated (acquire water into their structure) and oxidized by H_2O vapor to form Ti^{4+} on the substrate [13, 35]. Ti^{4+} is the most stable state because it is able to form an octet and ready to bond with other Ti^{4+} forming TiO_2. These initial nanorods can absorb titanium and oxygen from the medium to develop their growth process [35]. In this study, TiO_2 NRs will be synthesized with lower amount of HCl in hydrothermal solution compared with previous studies [6, 19]. This usability reduction of HCl not only contributes to decrease harmfulness of high acidity but also decrease the manufacturing cost of NRs synthesis.

2.5 Effect of seed layer on TiO_2 nanorods

Hyun Kim and Bee Lyong Yang [19] studied the growth of rutile titanium dioxide (TiO_2) nanorods on bare fluorine-doped The results illustrated that the average thickness of the seed layers was 140 nm composting of nanoparticles with 10-40 nm

ลิขสิทธิ์มหาวิทยาลัยเชียงใหม่
Copyright© by Chiang Mai University
All rights reserved

diameters. The surface of the SLs on FTO displayed lower roughness relative to bare FTO. The SLs was an anatase phase TiO_2 with an (101) diffraction peak. By hydrothermal method, lengths of performed nanorods were 1-2 μm. The diameter of NRs on the SLs was significantly reduced with the improvement of the density. The nanorods on the SLs had vertical-alinement with a high density. The TiO_2 NRs show a rutile tetragonal structure with (002) and (110) diffraction plane. NRs on seed layers and bare FTO are rutile tetragonal structure different in the dominate crystal plane. Dominate crystal plane of NRs on seed layers is (002) and (101) for NRs on FTO as illustrate in Figure 2.7 (b) The transparency of the nanorod on SLs was higher. Band gaps of the nanorods were about 2.95 eV compared to the bulk rutile phase with a 3.2 eV band gap. The difference is because of the NRs nanostructures having a larger surface area and smaller dimensions.

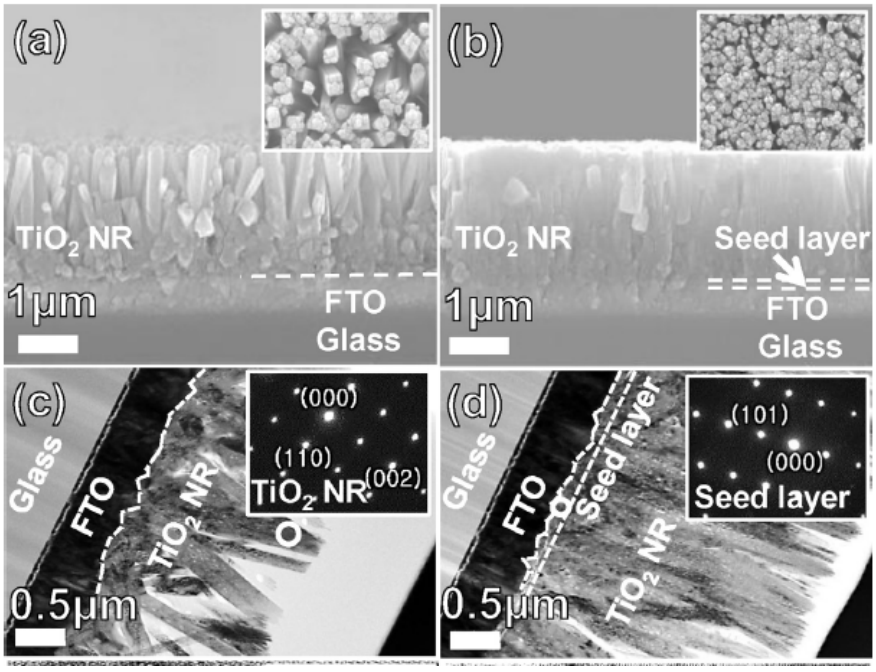

Figure 2.6 FE-SEM and TEM images of the TiO_2 NRs (a,c) and (b,d) are images of the TiO_2/FTO and TiO_2/SL/FTO [19]

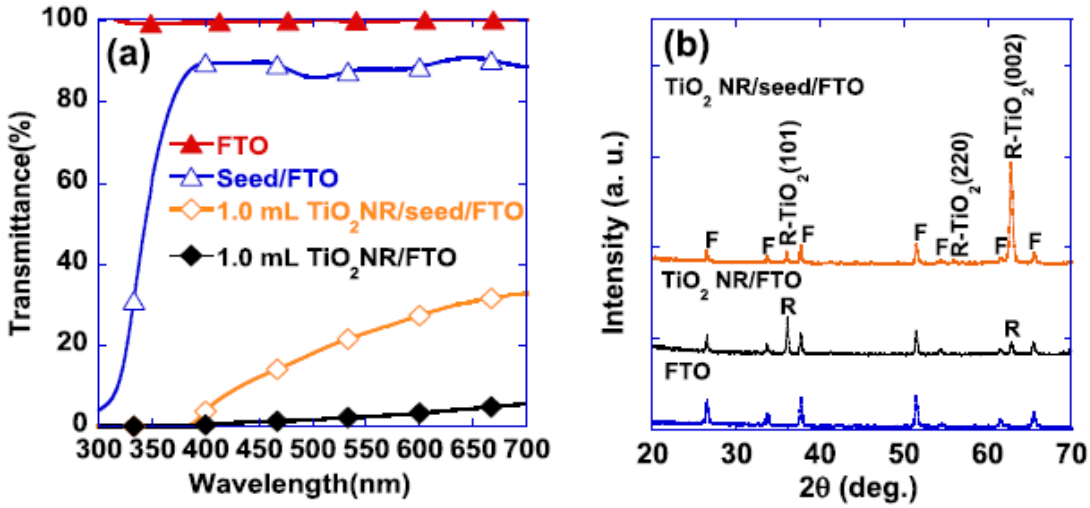

Figure 2. 7 (a) UV-Vis transmittance spectra of the bare FTO, SLs/ FTO, TiO_2 NRs/SLs/FTO and TiO_2 NRs/FTO grown by hydrothermal method using 1.0 mL of Ti precursor (b) X-ray diffraction patterns of the TiO_2 NRs/SLs/FTO, TiO_2 NRs/FTO, and FTO [19]

Jingyang Wang et al [3 6] studied seed layer effect on morphology and photo conversion efficiency of TiO_2 nanorods in dye-sensitized solar cells. In several of SLs concentration using $TiCl_4$ solution with various concentration (0.05 M, 0.1 M, 0.15 M, 0.2 M), the TiO_2 nanorods formation accomplished using hydrothermal method were reported. The grain size was increased and the surface roughness was decreased. Roughness of seeded-FTO reduced with the rise of $TiCl_4$ concentration because the higher $TiCl_4$ concentration is attributed to create the large TiO_2 nanoparticles. Therefore the orientation of the (002) rutile as increasing of $TiCl_4$ concentration with the greater vertical alignment. XRD patterns of NRs show TiO_2 rutile phase growth in [001] direction .

ลิขสิทธิ์มหาวิทยาลัยเชียงใหม่
Copyright© by Chiang Mai University
All rights reserved

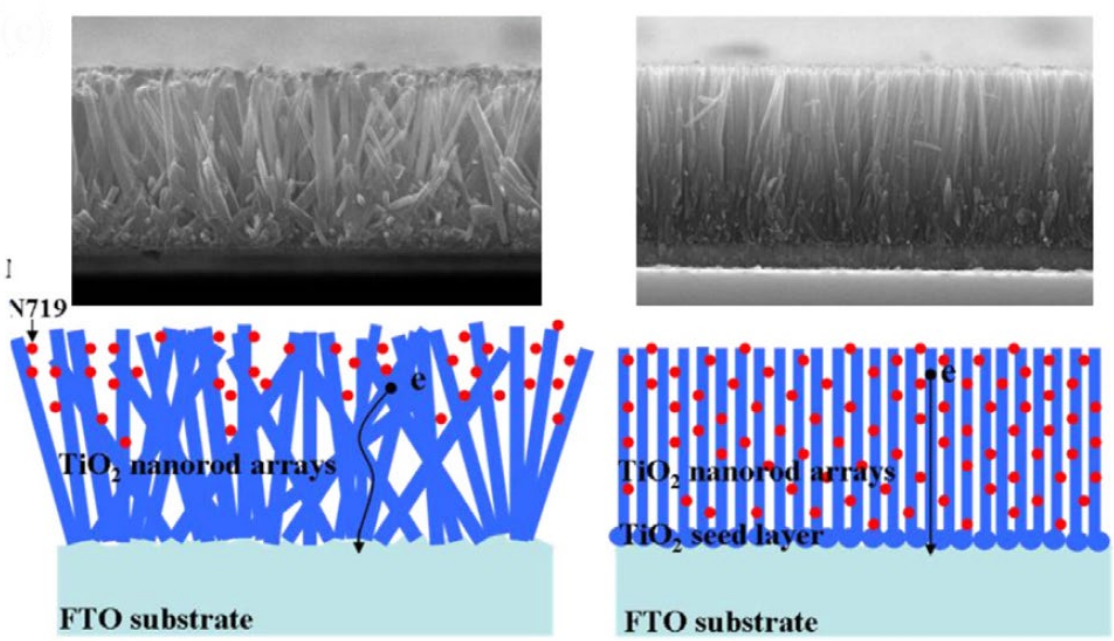

Figure 2.8 Diagram of the dye adsorption and electron transport of the TiO_2 NRs grown on bare and seeded-FTO [36]

SEM images display that TiO_2 NRs on SLs significantly decrease in diameter but increase in density with high regular orientation. TiO_2 NRs with SLs displayed higher reflection in the visible light region (420–750 nm), probably due to more efficiently incident light scattering from high density NRs. While the vertical alignment NRs result in the light path improvement thus, higher light harvest efficiency can be obtained. Moreover, the smaller TiO_2 NRs grown on SLs lead to lower resistance of the electron transfer at the interfaces [36].

ลิขสิทธิ์มหาวิทยาลัยเชียงใหม่
Copyright© by Chiang Mai University
All rights reserved

2.6 Application in Perovskite and dye-sensitized solar cell

2.6.1 Perovskite solar cells (PSCs)

Various observations report that TiO_2 nanorods (NRs) have capability more than conventional TiO_2 nanoparticles (NPs) since NPs consist of a great number of grain boundary leading to energy loss because of electrons scattering in grain boundary regions [6-8]. Recently, among one-dimensional (1D) TiO_2 nanostructures, TiO_2 NRs exhibit the remarkable electron transfer properties such as high photoelectrochemical (PEC) performance and high electron life time because they provide the direct electron pathway [12]. The prominent plane of NRs on SLs is (002). Photocurrent densities

measured for the nanorods primarily grown in the (002) orientation were larger [19]. Perovskite solar cell using TiO_2 NRs provide highest efficiency at 17.6 % (with current density (J_{sc}) 23.17 mA cm^{-2}) owing to the adequate NRs size and proper inter-rod spacing which are significant to promote electron transfer. While, too short NRs do not offer a sufficient number and density of heterojunctions for charge separation because of a low surface area. Too long and densely packed TNRs array results in poor penetration of perovskite and increases in the probability of electron-hole recombination.

2.6.2 Dye-sensitized solar cells (DSSCs)

The TiO_2 NRs without the SLs exhibits a low forward bias. TiO_2 NRs with result in shifting the onset to high bias. This can be attributed to the following reasons. First, the dense seeding layer can efficiently restrict charge recombination at the FTO surface. Second, recombination rate is decreased by fast electron transport in the vertical NRs at TiO_2 surface. The DSSCs based on TiO_2 NRs with a SLs exhibited higher short-circuit current density (J_{sc}) relative to the cell composing of bare NRs. The value of the J_{sc} using with SLs on FTO is increased from 2.60 to 4.91 mA/cm^2 due to the dye adsorption enhances with denser TiO_2 nanorods grown on SLs. DSSCs using NRs on $TiCl_4$ SLs can accomplish the maximum efficiency 2.55% which is higher than solar cell with NRs bare FTO (1.33% efficiency). It implied that the DSSCs based on the TiO_2 NRs grown on the SLs have the longer electron lifetime, which could reduce the electron recombination and lead to an improved performance of the cell.

ลิขสิทธิ์มหาวิทยาลัยเชียงใหม่
Copyright© by Chiang Mai University
All rights reserved